


The 3D-Printed PLGA Scaffolds Loaded with Bone Marrow-Derived Mesenchymal Stem Cells Augment the Healing of Rotator Cuff Repair in the Rabbits

Cell Transplantation
Volume 29: 1–13
© The Author(s) 2020
Article reuse guidelines:
sagepub.com/journals-permissions
DOI: 10.1177/0963689720973647
journals.sagepub.com/home/ccl


Peng Chen^{1,*}, Lei Cui^{2,*}, Sai Chuen Fu³, Li Shen⁴,
Wentao Zhang¹, Tian You¹, Tim-Yun Ong³, Yang Liu³ ,
Shu-Hang Yung³, and Changqing Jiang¹ 

Abstract

The healing of tendon–bone in the rotator cuff is featured by the formation of the scar tissues in the interface after repair. This study aimed to determine if the 3D-printed poly lactic-co-glycolic acid (PLGA) scaffolds loaded with bone marrow-derived mesenchymal stem cells (BMSCs) could augment the rotator cuff repair in the rabbits. PLGA scaffolds were generated by the 3D-printed technology; Cell Counting Kit-8 assay evaluated the proliferation of BMSCs; the mRNA and protein expression levels were assessed by quantitative real-time polymerase chain reaction and western blot, respectively; immunohistology evaluated the rotator cuff repair; biomechanical characteristics of the repaired tissues were also assessed. 3D-printed PLGA scaffolds showed good biocompatibility without affecting the proliferative ability of BMSCs. BMSCs–PLGA scaffolds implantation enhanced the cell infiltration into the tendon–bone junction at 4 weeks after implantation and improved the histology score in the tendon tissues after implantation. The mRNA expression levels of collagen I, III, tenascin, and biglycan were significantly higher in the scaffolds + BMSCs group at 4 weeks post-implantation than that in the scaffolds group. At 8 and 12 weeks after implantation, the biglycan mRNA expression level in the BMSCs–PLGA scaffolds group was significantly lower than that in the scaffolds group. BMSCs–PLGA scaffolds implantation enhanced collagen formation and increased collagen diameter in the tendon–bone interface. The biomechanical analysis showed that BMSCs–PLGA scaffolds implantation improved the biomechanical properties of the regenerated tendon. The combination of 3D-printed PLGA scaffolds with BMSCs can augment the tendon–bone healing in the rabbit rotator cuff repair model.

Keywords

tendon–bone, rotator cuff repair, 3D-printed PLGA scaffolds, BMSCs, collagen

¹ Department of Sports Medicine, Peking University Shenzhen Hospital, Shenzhen, Guangdong Province, China

² Clinical College of Peking University Shenzhen Hospital, Anhui Medical University, Hefei, China

³ Department of Orthopaedics and Traumatology, Faculty of Medicine, The Chinese University of Hong Kong, China

⁴ Department of Clinical Laboratory, Maternity and Child-Care Hospital of Pingshan District, Shenzhen, Guangdong Province, China

*Both the authors contributed equally to this article

Submitted: August 8, 2020. Revised: October 20, 2020. Accepted: October 26, 2020.

Corresponding Authors:

Changqing Jiang, Department of Sports Medicine, Peking University Shenzhen Hospital, Shenzhen, Guangdong Province, China.

Email: jcq-006@163.com

Shu-Hang Yung, Department of Orthopaedics and Traumatology, Faculty of Medicine, The Chinese University of Hong Kong, Hong Kong SAR, China.

Email: patrickyung@cuhk.edu.hk



Creative Commons Non Commercial CC BY-NC: This article is distributed under the terms of the Creative Commons Attribution-NonCommercial 4.0 License (<https://creativecommons.org/licenses/by-nc/4.0/>) which permits non-commercial use, reproduction and distribution of the work without further permission provided the original work is attributed as specified on the SAGE and Open Access pages (<https://us.sagepub.com/en-us/nam/open-access-at-sage>).

Introduction

The tendon–bone junction injuries in the rotator cuff commonly occur in workplaces and sports¹. The healing of tendon–bone in the rotator cuff is featured by the formation of scar tissues in the interface after repair. The incidence of re-tearing in the healed interface was relatively high, which affects more than 90% of patients under rotator cuff tendon repair^{2,3}. Up to date, graft materials including porcine dermal graft, autologous biceps tendon, small intestine submucosa, and human dermal graft have been used for mechanical augmentation, thereby, to improve the clinical outcomes of rotator cuff tendon–bone repair^{4–6}. However, grafting materials that are insufficient to promote the mechanical support may lead to high rates of surgical failure^{7,8}. Thereby, it is necessary to develop better graft materials to improve the clinical outcomes of the rotator cuff tendon–bone repair.

Bone marrow-derived mesenchymal stem cells (BMSCs) have been widely used in the cell-based tissue engineering, due to the self-renewal capacity and multipotent nature of these cells. BMSCs can differentiate into various types of cells such as adipocytes, chondrocytes, osteoblasts, and myocytes⁹. So far, several studies have addressed the application of BMSCs in the rotator cuff repair. Omi et al. showed that a multilayer xenograft tendon scaffold with BMSCs augmented the rotator cuff repair in a rat model¹⁰. Thangarajah et al. demonstrated that a demineralized cortical bone matrix combined with BMSCs augmented rotator cuff healing at 6 weeks after implantation in the chronic rotator cuff degeneration model¹¹. There is also evidence showing that BMSCs from the footprint could infiltrate into the repaired rotator cuff¹². In a case–control study, injection of BMSCs into the tendon-to-bone interface as an adjunctive therapy enhanced the healing rates and prevented further tears in the rotator cuff repair¹³. Collectively, BMSCs showed beneficial effects on augmenting the rotator cuff repair.

3D-printing is a newly developed technology. Recently, this technology has been used for generating biocompatible scaffolds in tissue regeneration¹⁴, as the 3D-printed scaffolds can be generated with a high degree of precision and complexity¹⁴. Park et al. showed that 3D bioprinted scaffold sleeves with MSCs augmented tendon-to-bone healing in anterior cruciate ligament reconstruction¹⁵. Wu et al. showed that 3D tendon scaffold could affect cell morphology and lead to desired gene expression toward tendon tissues¹⁶. Chou et al. found that combination of biodegradable collagen-loaded nanofibrous membranes and a 3D-printed bone-anchoring bolt enhanced the tendon–bone healing in a rabbit bone tunnel model¹⁷. However, the application of 3D-printed biocompatible scaffolds in the rotator cuff repair is sparse.

In this study, the 3D-printed poly lactic-co-glycolic acid (PLGA) biocompatible scaffolds were fabricated. The combination of 3D-printed PLGA scaffolds with BMSCs was applied in the tendon-to-bone healing in a model of rabbit rotator cuff repair. This study aimed to determine if the 3D-

printed PLGA scaffolds loaded with BMSCs could augment the rotator cuff repair in the rabbits.

Materials and Methods

Animals and Ethics Statement

All the animal experiments were under the approval of the Animal Ethics Committee of Peking University Shenzhen Hospital. The adult New Zealand rabbits (1.9 to 2.3 kg) were obtained from the Animal Center of Sun Yat-Sen University. All the animals were housed in separate metal cages with a relative humidity of $45\% \pm 10\%$ and a temperature of $24 \pm 2^\circ\text{C}$. The animals were provided free access to tap water and were fed with commercially available rabbit diet.

Isolation of BMSCs From the Rabbits

The isolation of BMSCs from the rabbits was carried out according to previous studies¹⁸. Briefly, New Zealand rabbits were killed by overdose of pentobarbitone (100 mg/kg, intraperitoneal [i.p.]), and the femurs and tibias were collected from the rabbits. BMSCs were collected by rinsing the diaphysis of femurs and tibias with phosphate-buffered saline (PBS) supplemented with 1% bovine serum albumin, penicillin (100 U/ml) and streptomycin (100 $\mu\text{g}/\text{ml}$). After further rinsing, the cells were resuspended in 5 ml PBS and were laid on the 5 ml Ficoll-Paque (GE Healthcare, Little Chalfont, UK). After that, the cells were centrifuged at $400 \times g$ for 30 min at room temperature, and cells were harvested from the plasma–Ficoll interface followed by rinsing with PBS for 3 times. The harvested BMSCs were cultivated in Dulbecco's modified Eagle medium (DMEM; Sigma-Aldrich, St Louis, MO, USA) supplemented with 10% fetal bovine serum (Sigma-Aldrich) at 37°C overnight, and floating cells were washed away the next day. All the attached BMSCs were cultured for further experimental analysis.

Alizarin Red Staining, Alcian Blue Staining, and Oil Red O Staining of Differentiated BMSCs

For Alizarin red staining, BMSCs were induced with 100 nM dexamethasone and 50 μM ascorbic acid-2-phosphate for 21 days, and the induced BMSCs were stained with 0.5% Alizarin red. For the Alcian blue staining, BMSCs were induced with 100 nM dexamethasone, 50 μM ascorbic acid-2-phosphate, and 10 ng/ml transforming growth factor-beta 1 for 21 days, and the BMSCs were stained with Alcian blue. For Oil red O staining, BMSCs were induced with 1 μM dexamethasone, 0.5 mM methyl-isobutyl-methyl-xanthine, 0.2 mM indomethacin, and 10 mg/ml insulin for 21 days, and induced BMSCs were stained with 0.2% oil red O.

Flow Cytometry Analysis of the Surface Markers of BMSCs

Flow cytometry analysis was performed to analyze the cell surface markers of BMSCs at passage 3 according to previous studies. Briefly, BMSCs were subjected to incubation with fluorescein isothiocyanate (FITC)-conjugated CD29+, CD90+, CD45+, and β 2m+ (Abcam, Cambridge, UK) at room temperature for 30 min in the dark. FITC-conjugated immunoglobulin isotype was used as negative controls. After rinsing with PBS, and BMSCs were resuspended in the PBS. The surface markers expressed in the BMSCs were analyzed by a flow cytometer (BD Biosciences, San Jose, CA, USA).

Fabrication of the 3D-Printed PLGA Scaffolds

The 3D-printed PLGA scaffolds were created using a 3DP system (Bioplotter; Envision TEC GmbH, Gladbeck, Germany) according to previous studies. The PLGA (molecular weight 50,000 to 75,000; poly lactic acid/poly glycolic acid 50:50) was purchased from Sigma-Aldrich. To fabricate the 3D-printed PLGA scaffolds, the PLGA powder was melted at 135°C and centrifuged at $100 \times g$ for 10 min at $\sim 140^\circ\text{C}$. The melted PLGA was dispensed via a 27-gauge metal needle to construct the 3D interconnected scaffolds. The dispensing temperature was 135°C, the pressure was $\sim 6,000$ kPa, and the XY dispense head speed was set at 80 mm/min. The microstructure of the scaffolds was examined by a scanning electron microscopy (SEM). The SMILE view software (JEOL, Tokyo, Japan) was used to determine the size of the pores in the scaffolds from the SEM images.

Cell Seeding Onto the 3D-Printed PLGA Scaffolds

For the BMSCs seeding, 3D-printed PLGA scaffolds were incubated with 70% ethanol for 12 h; after air-dried, the scaffolds were further immersed in DMEM for 7 days. After that, BMSCs (1×10^7 cells) were seeded onto the 3D-printed PLGA scaffolds. Scaffolds without BMSCs seeding were used as negative controls.

Cell Alignment and Elongation Assays

Alignment and elongation of BMSCs on the scaffolds or on the culture dishes were determined based on previously reported methods¹⁹.

Cell Counting Kit-8 Assay

The cell proliferative ability of BMSCs cultured on the culture dishes and 3D-printed PLGA scaffolds were analyzed using Cell Counting Kit-8 (CCK-8) assay (Beyotime, Beijing, China). Briefly, BMSCs seeded on the culture dishes or the scaffolds were cultured for 24, 48, 72, and 96 h, respectively. The BMSCs were harvested at the indicated time points and were incubated with the CCK-8 solution for 2 h

at 37°C. Cell proliferative ability was determined by measuring optical density values at the wavelength of 450 nm using a microplate reader (Bio-Tek).

Quantitative Real-Time Polymerase Chain Reaction

Total RNA from tendon tissues was isolated using the TRIzol reagent (Invitrogen, Carlsbad, CA, USA) according to the manufacturer's instruction. Total RNA was reversely transcribed into cDNA using the cDNA Synthesis Kit (Sigma-Aldrich). The real-time PCR was carried out on the ABI 7900 PCR detection system (Applied Biosystems, Foster City, CA, USA) using SYBR Premix Ex Taq II kit (Takara, Dalian, China). The primers for the respective genes were collagen I, forward, 5'-GATGGCCTGAAGCTCAA-3', reverse, 5'-GGTTTGTGAAGAGGCTG-3'; collagen III, forward, 5'-TTATAAACCAACCTCTTCCT-3', reverse, 5'-TATTATAGCACCATTGAGAC-3'; tenascin, forward, 5'-CGTGAAAACAATACCCGAGGC-3', reverse, 5'-GCCGTAGGAGAGTTCAATGCC-3'; Biglycan, forward, 5'-GATGGCCTGAAGCTCAA-3', reverse, 5'-GGTTTGTGAAGAGGCTG-3'; glyceraldehyde 3-phosphate dehydrogenase, forward, 5'-TCACCATCTCCAGGAGCGA-3', reverse, 5'-CACAATGCCGAAGTGTTCGT-3'. The relative expression levels of these genes were analyzed using comparative Ct method.

Rotator Cuff Repair Model in the Rabbits

The rotator cuff repair model in the rabbits was carried out according to previous studies with some modifications²⁰. Briefly, the animals were anesthetized using 3% isoflurane as vaporized in oxygen and delivered via a large animal cycling system (RWD Life Science, Shenzhen, China). Buprenorphine (0.05 mg/kg) was administered subcutaneously for analgesia before the surgery. All the operations were performed under the sterile conditions. After reaching general anesthesia, a longitudinal skin incision was made on the anterolateral aspect of the shoulder, and the rabbit deltoid was splitted and the rabbit supraspinatus was detached from its footprint. A 0.5-mm bone tunnel anterior to posterior via the greater tuberosity was created using a drill, and the supraspinatus tendon was detached from its insertion in the great tuberosity. A modified Mason-Allen technique was used to pass the nonabsorbable sutures in the tendon through the 0.5-mm bone tunnel. Before tying the suture, the 3D-printed PLGA scaffolds ($10 \times 5 \times 0.8$ mm) or the scaffolds ($10 \times 5 \times 0.8$ mm) seeded with BMSCs were implanted in the junction between the bone and tendon. Subcutaneous and skin sutures were performed to close the incision. After surgery, all the animals were allowed to move freely in their cages. Animals were given 0.05 mg/kg buprenorphine subcutaneously twice daily for consecutive 3 days to provide adequate analgesia. Intramuscular prophylactic antibiotic injections of penicillin G (400,000 U; Sigma-Aldrich) were given once a day for consecutive days. During the

postoperative time, the animal appetite, infection, bleeding, activity, and wound dehiscence were monitored every day. Both groups had 18 animals. At 4, 8, and 12 weeks after scaffolds implantation, the animals were killed by overdose of pentobarbitone (100 mg/kg, i.p.), and the regenerated tendon tissues were harvested for further experimental analysis.

Histology Analysis of the Tendon Tissues

The harvested tendon tissues were fixed with 4% paraformaldehyde in PBS and were embedded in paraffin. The paraffin-embedded tissues were cut into 5- μ m-thick slices in the coronal plane via the regenerative bone–tendon junction. The sections were stained with hematoxylin and eosin (H&E) or the Masson's trichrome staining according to previously reported methods²¹. The scoring criteria were as follows: 1, the insertion had continuity without bone ingrowth or fibrous tissues; 2, the insertion had continuity with fibrous tissue ingrowth but without fibrocartilage cells; 3, the insertion had continuity with fibrocartilage cells and fibrous tissue ingrowth but no tidemark; 4, the insertion had a tidemark, fibrocartilage cells, and fibrous tissue. The scoring was determined by two independent investigators.

Biomechanical Analysis of the Regenerated Tendon Tissues

The biomechanical characteristics were tested on an Electro-mechanical Universal Testing Systems (Instron, Norwood, MA, USA). Briefly, the regenerated tendon tissues were preloaded to 0.1 N and each tissue was loaded to failure at the rate of 50 mm/min. The final failure force and energy were recorded.

Analysis of Collagen Fibrils

The diameters of collagen fibrils were determined using transmission electron micrographs according to previously reported methods²². A minimum of 1,000 fibrils were analyzed from each sample.

Statistical Analysis

All the data analyses were performed using the GraphPad Prism V5.0 (GraphPad Software, La Jolla, CA, USA). All the experimental data were presented as mean \pm standard deviation. Significant differences between treatment groups were assessed using unpaired Student's *t*-test or two-way analysis of variance followed by Bonferroni's multiple comparison test. *P* < 0.05 was considered to be statistically significant.

Results

Characterization of the Isolated Rabbit BMSCs

Firstly, the surface biomarkers of the isolated BMSCs were analyzed using flow cytometry. As shown in Fig. 1A, the

CD45+ positive cells were 0.4%, β 2 M positive cells were 0.8%, while CD29+ and CD90+ positive cells were 98.1% and 93.8%, respectively. The Alizarin red staining showed the positive staining of the differentiated BMSCs, suggesting the osteogenic potential of the BMSCs (Fig. 1B). The Alcian blue staining showed the positive staining of the differentiated BMSCs, suggesting the chondrogenic potential of the BMSCs (Fig. 1C). Moreover, Oil red O staining showed the positive staining of the differentiated BMSCs, suggesting the adipogenic potential of the BMSCs (Fig. 1D).

Evaluation of the BMSCs Growth on the 3D-Printed PLGA Scaffolds

Figure 2A showed the top view and perspective view of the 3D-printed PLGA scaffolds. The mean pore size of the 3D-printed PLGA scaffolds was $861.12 \pm 21.87 \mu\text{m}$, and the porosity was $98.81\% \pm 0.04\%$ (Fig. 2B). The morphology of the BMSCs that cultured on the dishes and the scaffolds at 24 h after seeding was analyzed by H&E staining, as shown in Fig. 2C, D the elongated BMSCs in the culture dishes were randomly arranged, while the BMSCs seeded on the scaffolds were arranged in a parallel manner. In the inspection of the cell length, the BMSCs seeded on the scaffolds were markedly longer than the ones seeded on the culture dishes (Fig. 2E). The cell proliferative potential of these BMSCs was also analyzed using CCK-8 assay, and BMSCs seeded on the scaffolds showed similar proliferative potential to those seeded on the culture dishes (Fig. 2F).

Histology Analysis of the Repaired Tendon in the Rabbit

The implantation of the 3D-printed scaffolds in the injured area is shown in Fig. 3A. By the gross inspection, the scaffold remnant can exist up to 12 weeks after implantation. The scaffold remnant was seen at 4 (~50%) and 8 weeks (~30%), and was barely observed at 12 weeks (~5%) after implantation. At 4, 8, and 12 weeks after scaffolds implantation, the tendon tissues were collected for H&E staining. Figure 3B showed the morphology of the tendon tissues in the junction area at weeks after scaffolds implantation. The scaffolds seeded with BMSCs showed more infiltrated cells into the scaffolds area than those without BMSCs (Fig. 3B, D). Further analysis of the morphology in the outer zone and inner zone areas showed that the histology scores in the scaffolds + BMSCs group at 4, 8, and 12 weeks after implantation were significantly higher than that in the scaffolds group (Fig. 3C, E).

The Gene Expression Levels of Collagen I, Collagen III, TNC, and BGN in the Repaired Tendon Tissues of the Rabbit

The gene expression levels of collagen I, collagen III, TNC, and BGN in the tendon tissues at 4, 8, and 12 weeks after

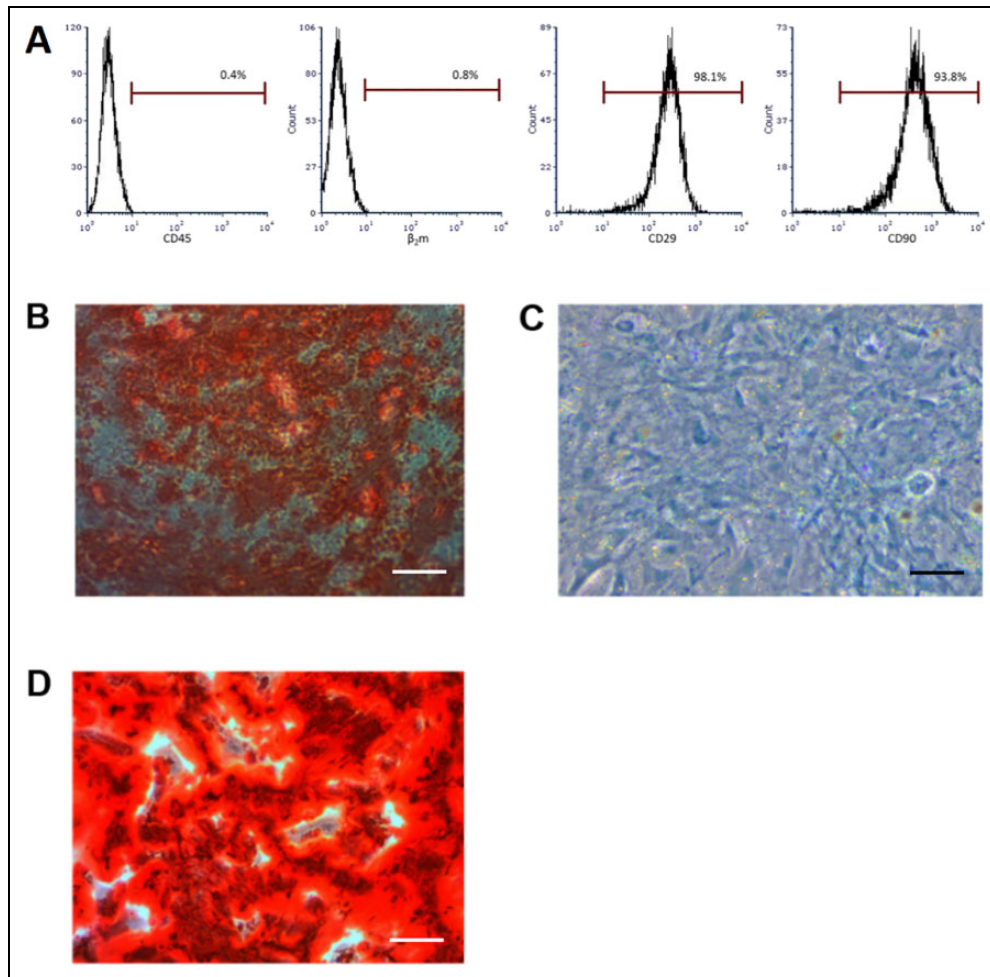


Figure 1. Characterization of the isolated rabbit BMSCs. (A) Flow cytometry analysis of the surface markers of CD45⁺, β₂m⁺, CD29⁺, and CD90⁺ in BMSCs. (B) Alizarin red staining of BMSCs. (C) Alcian blue staining of BMSCs. (D) Oil red O staining of BMSCs. Scale bar = 30 μm. BMSC: bone marrow-derived mesenchymal stem cell.

scaffolds implantation were analyzed by quantitative real-time polymerase chain reaction. At 4 weeks after implantation, the mRNA expression levels of collagen I, III, TNC, and BGN were significantly upregulated in the scaffolds + BMSCs group when compared to the scaffolds group (Fig. 4A–D). At 8 and 12 weeks after implantation, the scaffolds + BMSCs group showed downregulated BGN mRNA expression when compared to scaffolds group, whereas no significant difference in the collagen I, III, and TNC mRNA expression levels was detected between the two groups (Fig. 4A–D).

Masson Trichrome Staining of the Regenerative Tendon and Analysis of the Collagen Contents of the Regenerative Tendon

The Masson trichrome staining showed that more collagens and fibrocartilage cells in both inner zone and outer zone were observed in the scaffolds + BMSCs group at 4, 8, and 12 weeks after implantation when compared to scaffolds group (Fig. 4A). Collagens and fibrocartilage cells were

more abundant in the inner zone than that in the outer zone from the Scaffolds + BMSCs group at 8 and 12 weeks after implantation (Fig. 5A). Further analysis showed that no significant difference was detected in the collagen contents of the tendon tissues at 4, 8, and 12 weeks after scaffold implantation between the two groups (Fig. 5B).

Collagen Fibrils Analysis and Biomechanical Analysis of the Regenerative Tendon Tissues

In the analysis of collagen fibrils, the collagen diameter was mainly 35 to 35 nm in the scaffolds group at 8 weeks after implantation, where the collagen diameter was mainly 45 to 60 nm in the scaffolds + BMSCs group at 8 weeks after implantation (Fig. 6A). At 12 weeks after scaffold implantation, the collagen diameter in both groups were 45 to 55 nm (Fig. 6B). At 8 weeks after implantation, the mean diameters in the scaffolds + BMSCs group were significantly higher than that in the scaffolds group (Fig. 6C); at 12 weeks after scaffold implantation, no significant difference in the

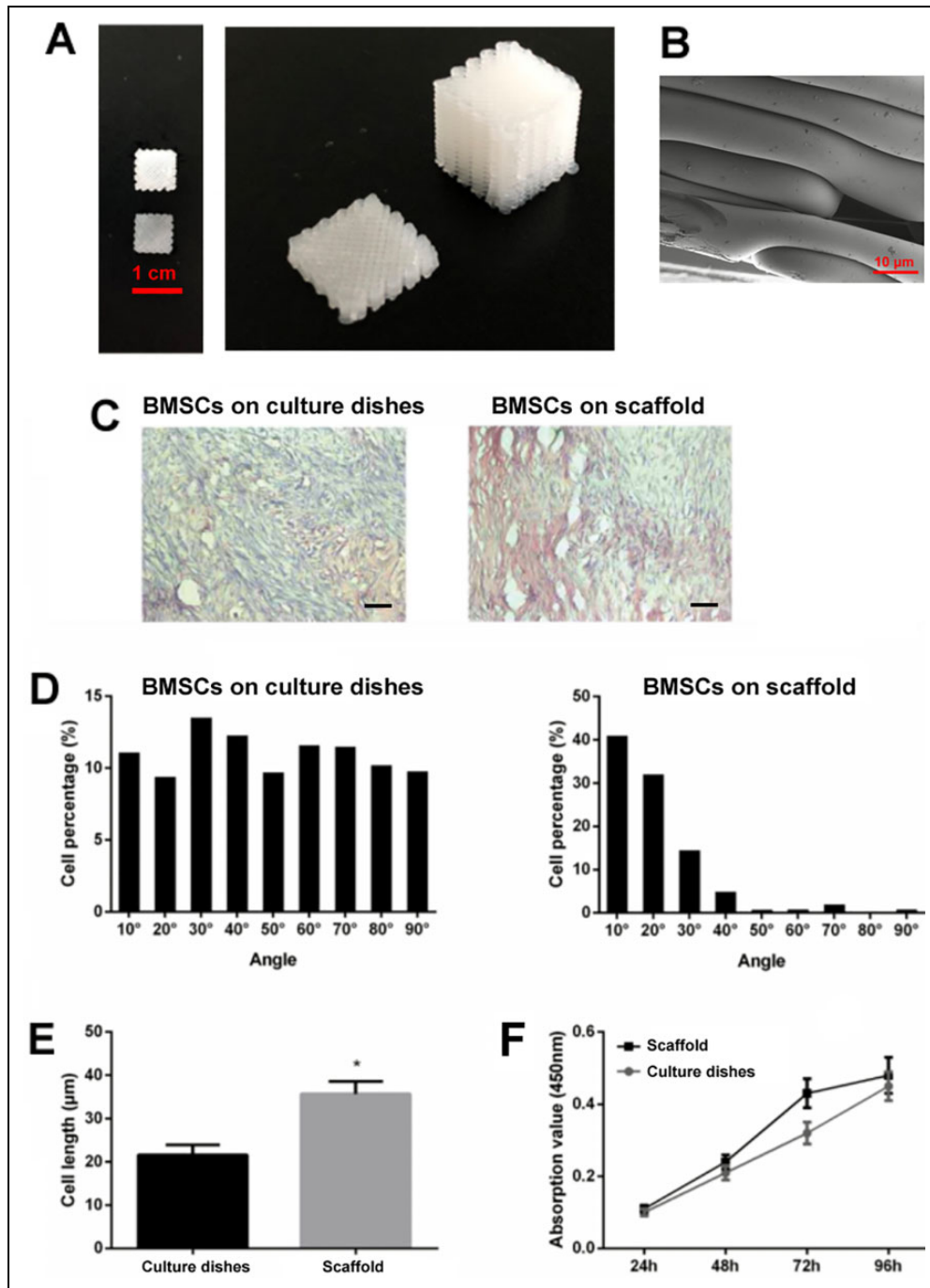


Figure 2. Evaluation of the BMSCs growth on the 3D-printed PLGA scaffold. (A) The morphology of the 3D-printed PLGA scaffold. Left panel showed the top view of the 3D-printed PLGA scaffold, right panel showed that perspective view of the 3D-printed PLGA scaffold. (B) SEM. (C) Typical hematoxylin and eosin staining showed the morphology and arrangement of BMSCs on the culture dishes or on the scaffolds at 24 h after seeding. (D) Angular distributions of BMSCs on the culture dishes or the scaffolds at 24 h after seeding. (E) Cell length of the BMSCs on the culture dishes or the scaffolds at 24 h after seeding (unpaired Student's *t*-test). (F) Cell proliferative ability of BMSCs on the culture dishes or the scaffolds at 24 h after seeding (two-way analysis of variance followed by Bonferroni's multiple comparison test). $N = 3$. * $P < 0.05$. Scale bar = 30 μm .

BMSC: bone marrow-derived mesenchymal stem cell; PLGA: poly lactic-co-glycolic acid.

collagen diameter was detected between the two groups (Fig. 6D). Further analysis of the biomechanical properties of the regenerative tendon tissues showed that the failure force and

energy of the tendon tissues were significantly higher in the scaffolds + BMSCs group than in the scaffolds group (Fig. 6E, F) and all the failures occur at the tendon–bone interface.

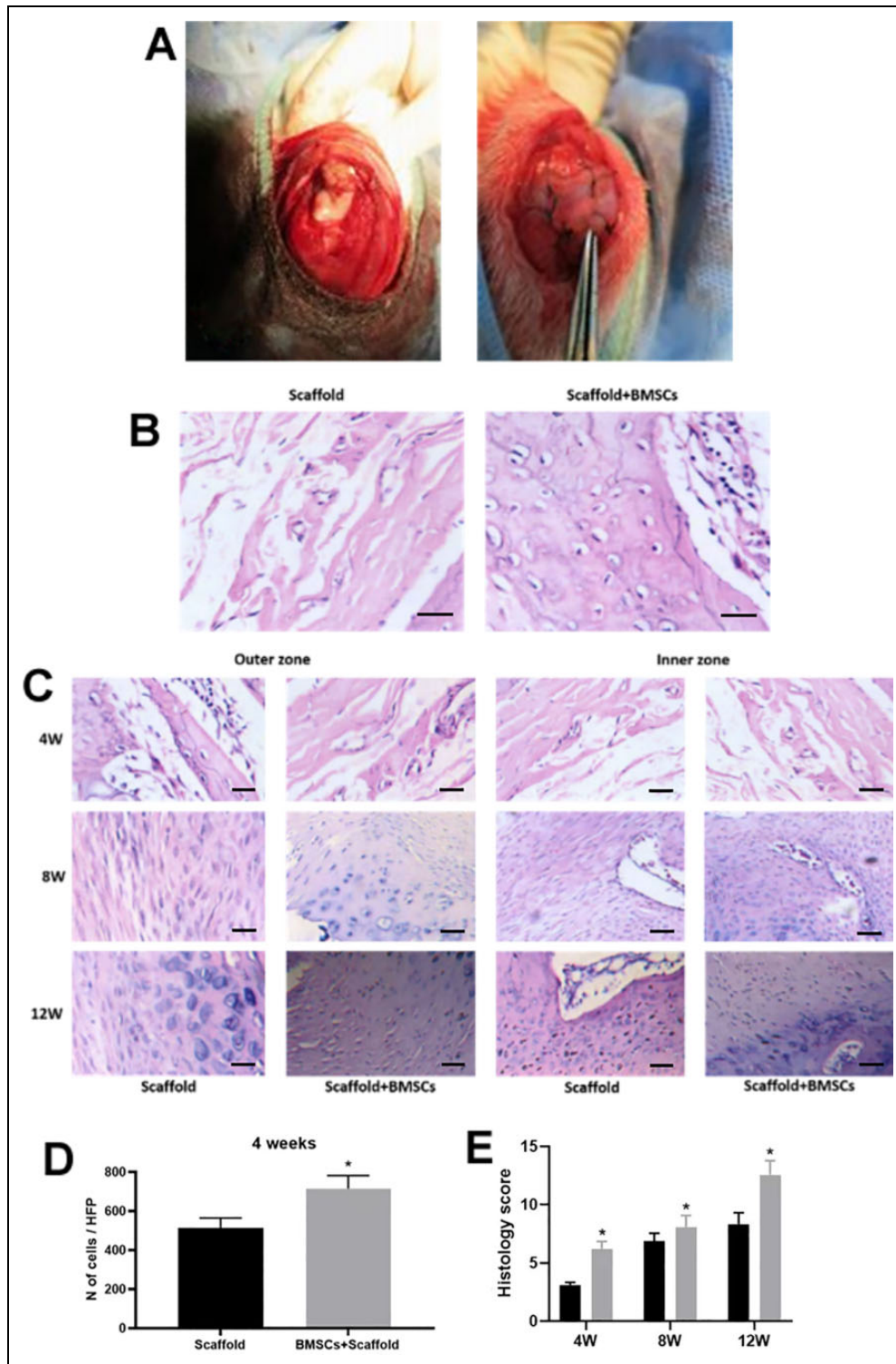


Figure 3. Histology analysis of the repaired tendon in the rabbit. (A) Images showed the implantation of 3D-printed scaffolds in the surgically excised tendon. (B) H&E staining of the regenerative tendon in the junction. (C) H&E staining of the regenerative tendon in the outer and inner zones at 4, 8, and 12 weeks after scaffolds implantation. (D) Number of infiltrated cells within the scaffolds was evaluated at 4 weeks after scaffolds implantation (unpaired Student's *t*-test). (E) Histological score of the regenerative tendon at 4, 8, and 12 weeks after scaffolds implantation (two-way analysis of variance followed by Bonferroni's multiple comparison test). $N = 6$. * $P < 0.05$. Scale bar = 30 μm . BMSC: bone marrow-derived mesenchymal stem cell; H&E: hematoxylin and eosin; w: weeks.

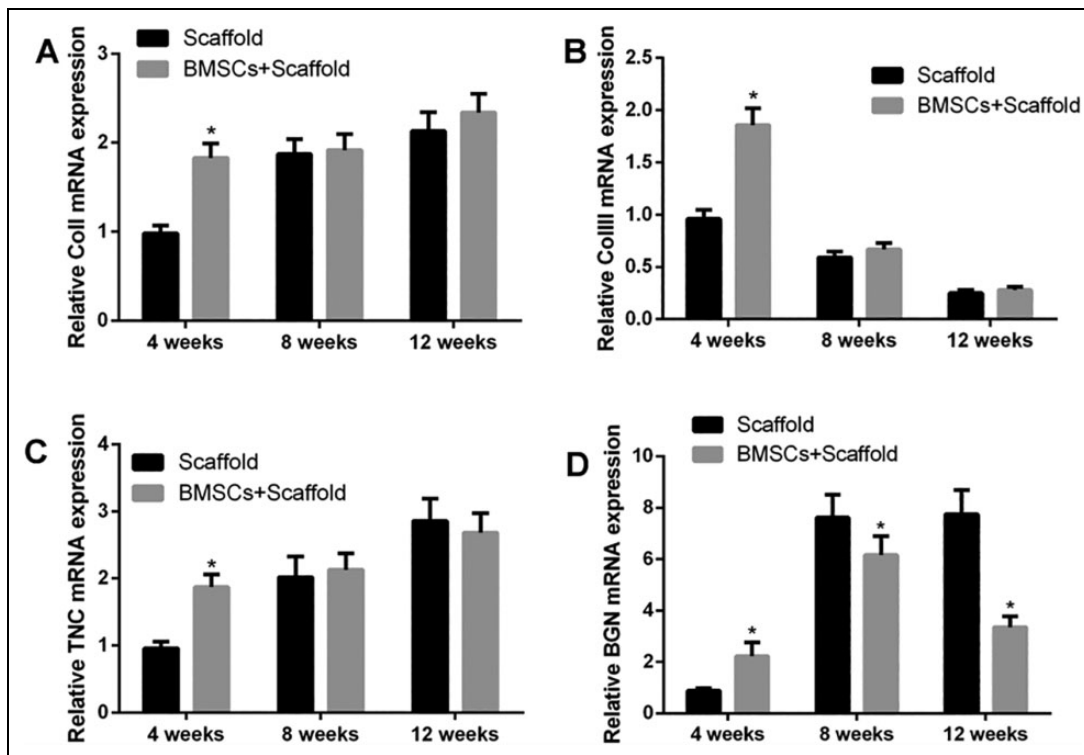


Figure 4. The gene expression levels of collagen I, collagen III, TNC, and BGN in the repaired tendon tissues of the rabbit. (A) Collagen I, (B) collagen III, (C) TNC, and (D) BGN mRNA expression levels in the tendon tissues at 4, 8, and 12 weeks after scaffold implantation were evaluated using quantitative real-time polymerase chain reaction analysis (two-way analysis of variance followed by Bonferroni's multiple comparison test). $N = 6$. * $P < 0.05$.

BMSC: bone marrow-derived mesenchymal stem cell.

Discussion

The tendon–bone injury in the rotator cuff affects a large population¹. Due to the high incidence of re-tearing in rotator cuff repair, the rates of surgical failure are relatively high². Recently, BMSCs have been widely used in the tissue regeneration, due to the self-renewal capacity and multipotent nature of these cells⁹. The application of 3D print technology has produced biocompatible scaffolds with a high degree of precision and complexity. In the present study, we first isolated the BMSCs from the rabbits, and these cells exhibited characteristics of multipotency with osteogenic, chondrogenic, and adipogenic potentials. The 3D-printed PLGA scaffolds showed good biocompatibility without affecting the proliferative ability of seeded BMSCs. The *in vivo* studies showed that the combination of 3D-printed PLGA scaffolds with BMSCs can augment the tendon–bone healing in the model of rabbit rotator cuff repair.

BMSCs have been shown to possess self-renewing and multipotent properties, and preparation and culture of BMSCs are not complicated, which makes BMSCs ideal candidates for the tendon tissues engineering²³. Various strategies such as mechanical stimulation, tenogenic gene transfection, physical topography induction, and decellularized

tendon matrices have been developed to facilitate the BMSC teno-lineage differentiation²³. The presence of a tendinous matrix was effective to promote BMSCs-mediated repair of Achilles tendon²⁴. The proper topography of the scaffolds could promote the induction of teno-lineage differentiation in an Achilles tendon injury model²⁵. Application of the aligned nanofibers can also induce the tendon-like tissue regeneration²⁶. In our study, we fabricated the customized scaffolds by using the 3D-print technology, and the 3D-printed scaffolds consisted of fully interconnected pores. The 3D-printed PLGA scaffolds allowed the growing of BMSCs and augmented the tendon-to-bone healing in the rotator cuff repair. These results suggested that 3D-printed PLGA scaffolds may be a good graft for harboring the BMSCs for tissue engineering.

The PLGA possesses good biodegradable and biocompatible characteristics and has been approved by Food and Drug Administration for its clinical application in the bone tissues engineering²⁷. PLGA can be used as the carrier for medical materials including BMSCs²⁷. Studies found that BMP-7-loaded fibrous PLGA scaffolds with synovium-resident MSCs induced proteoglycan and collagen II and enhanced thick hyaline cartilage formation in the articular cartilage repair²⁸. The coating of nano-hydroxyapatite with

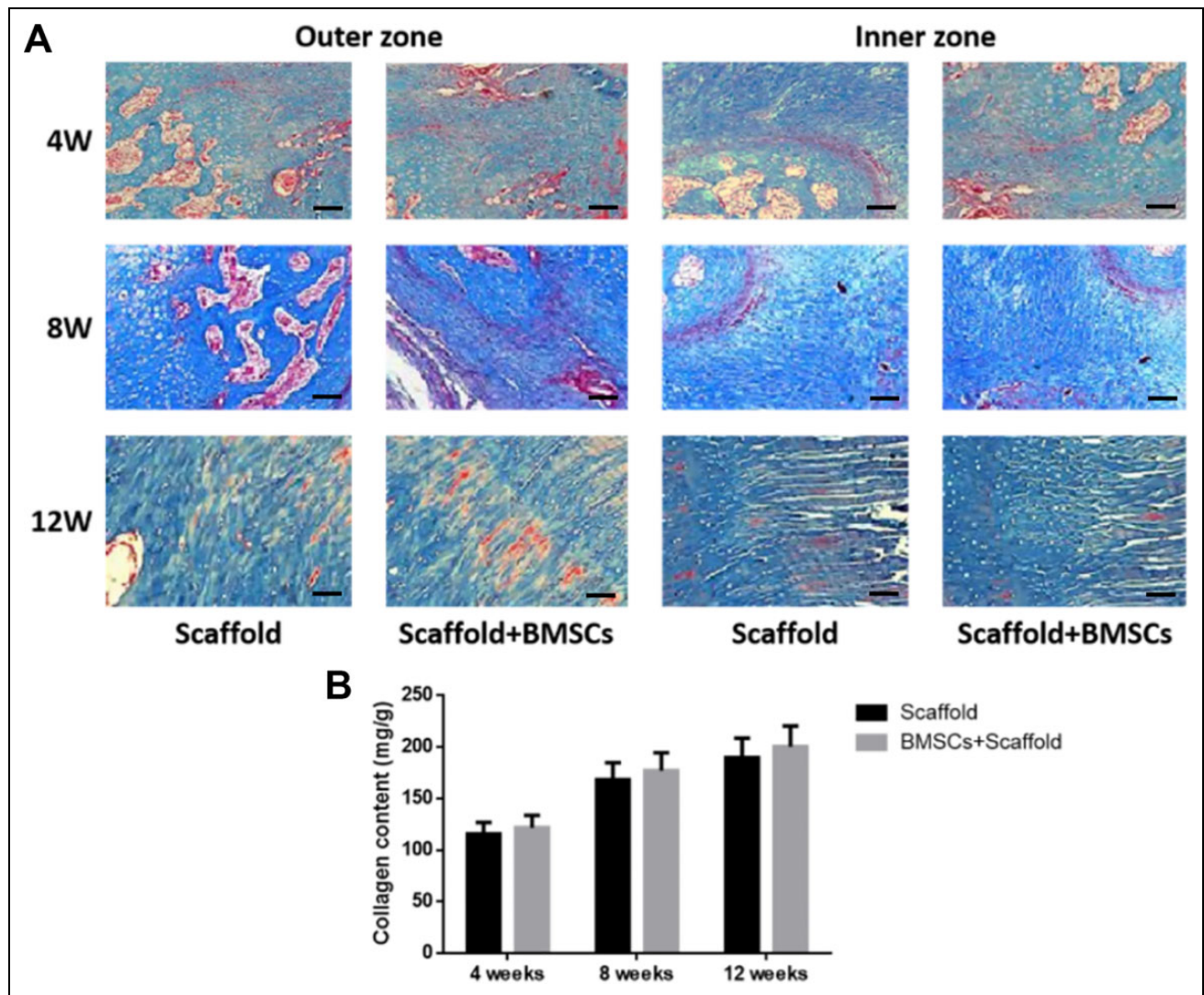


Figure 5. Masson trichrome staining of the regenerative tendon and analysis of the collagen contents of the regenerative tendon. (A) Masson trichrome staining of the regenerative tendon at 4, 8, and 12 weeks after scaffolds implantation. (B) Collagen contents analysis of the regenerative tendon at 4, 8, and 12 weeks after scaffolds implantation (two-way analysis of variance followed by Bonferroni's multiple comparison test). $N = 6$. Scale bar = 30 μm . BMSC: bone marrow-derived mesenchymal stem cell; W: weeks.

multilayer deposition on the PLGA scaffolds could promote the BMSCs' osteogenic differentiation via upregulating osteogenic marker genes²⁹. Knitted PLGA scaffolds seeded with BMSCs were effective to promote the regeneration and repair in the rabbit Achilles tendon³⁰. In the present study, the BMSCs seeded on the 3D-printed PLGA scaffolds showed similar proliferative potential to the ones on the culture dishes, suggesting that the scaffolds do not affect the proliferative potential of BMSCs. Cellular networks rely on interconnected pathways for nutrient transportation, cell signaling, and proliferation in the extracellular matrix (ECM)³¹. The 3D-printed PLGA scaffolds have a nanofibrous structure that bears a close resemblance to native ECM³², which may enhance the cell infiltration of BMSCs in the present

study. Studies demonstrated that the nanofiber alignment within the scaffolds could regulate tendon stem cell orientation and induce specific teno-lineage differentiation²⁶, and the fibers aligned with the 3D-printed PLGA scaffolds from the present study may also exert enhanced effects on the teno-lineage differentiation.

In this study, we examined the gene expression profiles of collagen I, II, tenascin, and biglycan in the process of the rotator cuff repair. At 4 weeks after implantation, expression levels of collagen I and III mRNA were upregulated in the BMSCs + scaffolds group when compared to scaffolds group. At 8 and 12 weeks, the expression of collagen I mRNA continuously elevated, while collagen III mRNA expression was gradually decreased. The expressing pattern

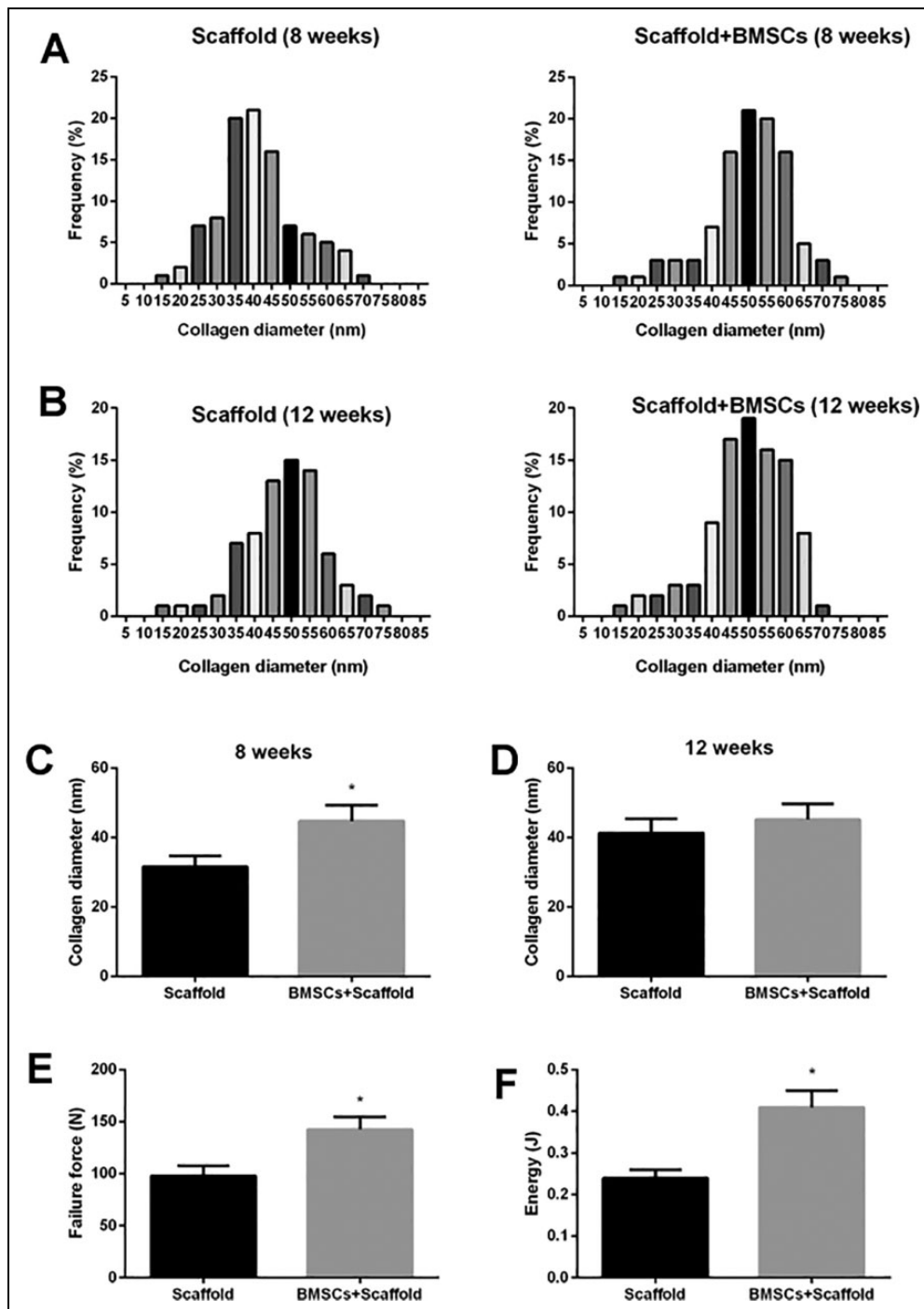


Figure 6. Collagen fibrils analysis and biomechanical analysis of the regenerative tendon. (A) Analysis of collagen diameter distribution of the regenerative tendon at 8 weeks after scaffolds implantation. (B) Analysis of collagen diameter distribution of the regenerative tendon at 12 weeks after scaffolds implantation. (C) collagen diameter of the regenerative tendon at 8 weeks after scaffolds implantation (unpaired Student's *t*-test). (D) collagen diameter of the regenerative tendon at 12 weeks after scaffolds implantation (unpaired Student's *t*-test). (E and F) Biomechanical analysis (failure force and energy) of the regenerative tendon at 12 weeks after scaffolds implantation (unpaired Student's *t*-test). $N = 6$. * $P < 0.05$.

BMSC: bone marrow-derived mesenchymal stem cell.

of collagen I and III in this study consists with the natural healing process of the tendon and is key for maintaining the tendon structure and function³³. In the healing of rotator cuff tears, studies demonstrated that repair tissues mainly

produced collagen III in the early phase of healing, and collagen I subsequently increased and replaced collagen III³⁴. Tenascin is an ECM protein and mainly located in the musculoskeletal regions, and it plays an important role in

transmitting mechanical forces from one tissue component to another³⁵. In a rabbit tendon–bone interface repair model, tenascin mRNA expression was increased with the healing process³⁶, and our study showed the similar findings that tenascin mRNA expression level was continuously elevated over time after the scaffolds implantation, which was consistent with the results revealed by Chainani et al.³⁷. Biglycan is a type of small leucine-rich proteoglycan and is upregulated after tendon injury³⁸. On the other hand, the presence of the biglycan is crucial for initial healing and biglycan protein degraded over time during the healing process in the tendon injury³⁹. We consistently showed that biglycan was upregulated at 4 weeks after implantation and the expression level was gradually decreased at 8 and 12 weeks after implantation. In the view of collagen fibrils and biomechanical properties, implantation of BMSC-seeded scaffolds showed greater diameter of collagen fibrils and better mechanical properties at 12 weeks post-implantation when compared to implantation of the scaffolds alone, which were consistent with improved histology score. Collectively, these results suggest that the 3D-printed PLGA scaffolds with BMSCs promoted the healing of the rotator cuff repair in the rabbits.

Several limitations still require our attention in the present study. First, the present study may lack a more clinically relevant control or cell-scaffold treatment, which should be considered in our future studies. Secondly, the present study has not examined chronic lymphocytic infiltrate or macrophages or foreign body reactions after scaffold implantation, which may further have great impact on the tendon bone-healing process. Future studies may consider the investigation to further uncover the mechanism underlying the scaffold-mediated tendon–bone repair. Thirdly, the present study used the nonabsorbable sutures, and other studies may compare the other types of sutures including total absorbable and partial absorbable sutures, as the suture absorbability affects the rotator cuff healing in the rabbit rotator cuff repair model⁴⁰. Fourthly, the degradation of scaffold has not been assessed in detail, and future studies should also consider the degrading dynamics of the scaffolds, in order to fully uncover the potential application of this technique.

Conclusions

In conclusion, the present study showed that the 3D-printed PLGA scaffolds loaded with BMSCs augmented the healing at the tendon–bone interface in a rabbit rotator cuff repair model. The application of BMSCs-loaded 3D-printed PLGA may represent a novel strategy to improve the clinical outcomes of the rotator cuff repair.

Authors Contributions

SY and CJ directed the experimental study. PC, LC, SCF, and LS performed the experiments, analyzed the data, and wrote the manuscript. WZ and TY provided technical support. TO and YL

contributed to the language editing. All the authors approved the manuscript for submission.

Data Availability Statement

All the data generated in the manuscript are available upon reasonable request.

Ethical Approval

Ethical Approval is not applicable for this article.

Statement of Human and Animal Rights

This article does not contain any studies with human subjects or animals.

Statement of Informed Consent

There are no human subjects in this article and informed consent is not applicable.

Declaration of Conflicting Interests


The author(s) declared no potential conflicts of interest with respect to the research, authorship, and/or publication of this article.

Funding

The author(s) disclosed receipt of the following financial support for the research, authorship, and/or publication of this article: This work is partly supported by Science and Technology Project of Shenzhen (Grant No. JCYJ20180228175214999) and Sanming Project of Medicine in Shenzhen (Grant No. SZSM201612078).

ORCID iDs

Yang Liu  <https://orcid.org/0000-0003-3831-7153>

Changqing Jiang  <https://orcid.org/0000-0002-8616-7527>

References

1. Benjamin M, Toumi H, Ralphs JR, Bydder G, Best TM, Milz S. Where tendons and ligaments meet bone: attachment sites ('entheses') in relation to exercise and/or mechanical load. *J Anat.* 2006;208(4):471–490.
2. Nikolaidou O, Migkou S, Karamalis C. Rehabilitation after rotator cuff repair. *Open Orthop J.* 2017;11:154–162.
3. Thigpen CA, Shaffer MA, Gaunt BW, Leggin BG, Williams GR, Wilcox RB 3rd. The American society of shoulder and elbow therapists' consensus statement on rehabilitation following arthroscopic rotator cuff repair. *J Shoulder Elbow Surg.* 2016;25(4):521–535.
4. Gillespie RJ, Knapik DM, Akkus O. Biologic and synthetic grafts in the reconstruction of large to massive rotator cuff tears. *J Am Acad Orthop Surg.* 2016;24(12):823–828.
5. Lewington MR, Ferguson DP, Smith TD, Burks R, Coady C, Wong IH. Graft utilization in the bridging reconstruction of irreparable rotator cuff tears: a systematic review. *Am J Sports Med.* 2017;45(13):3149–3157.
6. Murthi AM, Lankachandra M. Technologies to augment rotator cuff repair. *Orthop Clin North Am.* 2019;50(1):103–108.
7. Ahmad Z, Henson F, Wardale J, Noorani A, Tytherleigh-Strong G, Rushton N. Review article: regenerative techniques

- for repair of rotator cuff tears. *J Orthop Surg (Hong Kong)*. 2013;21(2):226–231.
8. McCormack RA, Shreve M, Strauss EJ. Biologic augmentation in rotator cuff repair—should we do it, who should get it, and has it worked?. *Bull Hosp Jt Dis*. 2014;72(1):89–96.
 9. Colter DC, Sekiya I, Prockop DJ. Identification of a subpopulation of rapidly self-renewing and multipotential adult stem cells in colonies of human marrow stromal cells. *Proc Natl Acad Sci U S A*. 2001;98(14):7841–7845.
 10. Omi R, Gingery A, Steinmann SP, Amadio PC, An KN, Zhao C. Rotator cuff repair augmentation in a rat model that combines a multilayer xenograft tendon scaffold with bone marrow stromal cells. *J Shoulder Elbow Surg*. 2016;25(3):469–477.
 11. Thangarajah T, Sanghani-Kerai A, Henshaw F, Lambert SM, Pendegrass CJ, Blunn GW. Application of a demineralized cortical bone matrix and bone marrow-derived mesenchymal stem cells in a model of chronic rotator cuff degeneration. *Am J Sports Med*. 2018;46(1):98–108.
 12. Kida Y, Morihara T, Matsuda K, Kajikawa Y, Tachiiri H, Iwata Y, Sawamura K, Yoshida A, Oshima Y, Ikeda T, Fujiwara H, et al. Bone marrow-derived cells from the footprint infiltrate into the repaired rotator cuff. *J Shoulder Elbow Surg*. 2013;22(2):197–205.
 13. Hernigou P, Flouzat Lachaniette CH, Delambre J, Zilber S, Duffiet P, Chevallier N, Rouard H. Biologic augmentation of rotator cuff repair with mesenchymal stem cells during arthroscopy improves healing and prevents further tears: a case-controlled study. *Int Orthop*. 2014;38(9):1811–1818.
 14. Do AV, Khorsand B, Geary SM, Salem AK. 3D printing of scaffolds for tissue regeneration applications. *Adv Healthc Mater*. 2015;4(12):1742–1762.
 15. Park SH, Choi YJ, Moon SW, Lee BH, Shim JH, Cho DW, Wang JH. Three-dimensional bio-printed scaffold sleeves with mesenchymal stem cells for enhancement of tendon-to-bone healing in anterior cruciate ligament reconstruction using soft-tissue tendon graft. *Arthroscopy*. 2018;34(1):166–179.
 16. Wu Y, Wong YS, Fuh JY. Degradation behaviors of geometric cues and mechanical properties in a 3D scaffold for tendon repair. *J Biomed Mater Res A*. 2017;105(4):1138–1149.
 17. Chou YC, Yeh WL, Chao CL, Hsu YH, Yu YH, Chen JK, Liu SJ. Enhancement of tendon-bone healing via the combination of biodegradable collagen-loaded nanofibrous membranes and a three-dimensional printed bone-anchoring bolt. *Int J Nanomedicine*. 2016;11:4173–4186.
 18. Chen P, Cui L, Chen G, You T, Li W, Zuo J, Wang C, Zhang W, Jiang C. The application of BMP-12-overexpressing mesenchymal stem cells loaded 3D-printed PLGA scaffolds in rabbit rotator cuff repair. *Int J Biol Macromol*. 2019;138:79–88.
 19. Wang ZY, Teo EY, Chong MSK, Zhang QY, Lim J, Zhang ZY, Hong MH, Thian ES, Chan JKY, Teoh S-h. Biomimetic three-dimensional anisotropic geometries by uniaxial stretch of poly(ϵ -caprolactone) films for mesenchymal stem cell proliferation, alignment, and myogenic differentiation. *Tissue Engineering Part C Methods*. 2013;19(7):538–549.
 20. Gao Y, Zhang Y, Lu Y, Wang Y, Kou X, Lou Y, Kang Y. TOB1 Deficiency enhances the effect of bone marrow-derived mesenchymal stem cells on tendon-bone healing in a rat rotator cuff repair model. *Cell Physiol Biochem*. 2016;38(1):319–329.
 21. Klontzas ME, Kenanidis EI, Heliotis M, Tsiridis E, Mantalaris A. Bone and cartilage regeneration with the use of umbilical cord mesenchymal stem cells. *Expert Opin Biol Ther*. 2015;15(11):1541–1552.
 22. Achari Y, Chin JW, Heard BJ, Rattner JB, Shrive NG, Frank CB, Hart DA. Molecular events surrounding collagen fibril assembly in the early healing rabbit medial collateral ligament—failure to recapitulate normal ligament development. *Connect Tissue Res*. 2011;52(4):301–312.
 23. Yin Z, Guo J, Wu TY, Chen X, Xu LL, Lin SE, Sun YX, Chan KM, Ouyang H, Li G. Stepwise differentiation of mesenchymal stem cells augments tendon-like tissue formation and defect repair *in vivo*. *Stem Cells Transl Med*. 2016;5(8):1106–1116.
 24. Yin Z, Chen X, Zhu T, Hu JJ, Song HX, Shen WL, Jiang LY, Heng BC, Ji JF, Ouyang HW. The effect of decellularized matrices on human tendon stem/progenitor cell differentiation and tendon repair. *Acta Biomater*. 2013;9(12):9317–9329.
 25. Yin Z, Chen X, Song HX, Hu JJ, Tang QM, Zhu T, Shen WL, Chen JL, Liu H, Heng BC, Ouyang HW. Electrospun scaffolds for multiple tissues regeneration *in vivo* through topography dependent induction of lineage specific differentiation. *Biomaterials*. 2015;44:173–185.
 26. Yin Z, Chen X, Chen JL, Shen WL, Hieu Nguyen TM, Gao L, Ouyang HW. The regulation of tendon stem cell differentiation by the alignment of nanofibers. *Biomaterials*. 2010;31(8):2163–2175.
 27. Li YH, Wang ZD, Wang W, Ding CW, Zhang HX, Li JM. The biocompatibility of calcium phosphate cements containing alendronate-loaded PLGA microparticles *in vitro*. *Exp Biol Med (Maywood)*. 2015;240(11):1465–1471.
 28. Kim HJ, Han MA, Shin JY, Jeon JH, Lee SJ, Yoon MY, Kim HJ, Choi EJ, Do SH, Yang VC, He H, et al. Intra-articular delivery of synovium-resident mesenchymal stem cells via BMP-7-loaded fibrous PLGA scaffolds for cartilage repair. *J Control Release*. 2019;302:169–180.
 29. Kong J, Wei B, Groth T, Chen Z, Li L, He D, Huang R, Chu J, Zhao M. Biomimetic mineralization improves mechanical and osteogenic properties of multilayer-modified PLGA porous scaffolds. *J Biomed Mater Res A*. 2018;106(10):2714–2725.
 30. Ouyang HW, Goh JC, Thambyah A, Teoh SH, Lee EH. Knitted poly-lactide-co-glycolide scaffold loaded with bone marrow stromal cells in repair and regeneration of rabbit Achilles tendon. *Tissue Eng*. 2003;9(3):431–439.
 31. Stratton S, Shelke NB, Hoshino K, Rudraiah S, Kumbar SG. Bioactive polymeric scaffolds for tissue engineering. *Bioact Mater*. 2016;1(2):93–108.
 32. Wu J, Hong Y. Enhancing cell infiltration of electrospun fibrous scaffolds in tissue regeneration. *Bioact Mater*. 2016;1(1):56–64.
 33. Williams IF, McCullagh KG, Silver IA. The distribution of types I and III collagen and fibronectin in the healing equine tendon. *Connect Tissue Res*. 1984;12(3-4):211–227.

34. Hirose K, Kondo S, Choi HR, Mishima S, Iwata H, Ishiguro N. Spontaneous healing process of a supraspinatus tendon tear in rabbits. *Arch Orthop Trauma Surg.* 2004;124(6):374–377.
35. Jarvinen TA, Kannus P, Jarvinen TL, Jozsa L, Kalimo H, Jarvinen M. Tenascin-C in the pathobiology and healing process of musculoskeletal tissue injury. *Scand J Med Sci Sports.* 2000; 10(6):376–382.
36. Qian S, Wang Z, Zheng Z, Ran J, Zhu J, Chen W. A Collagen and silk scaffold for improved healing of the tendon and bone interface in a rabbit model. *Med Sci Monit.* 2019;25:269–278.
37. Chainani A, Hippensteel KJ, Kishan A, Garrigues NW, Ruch DS, Guilak F, Little D. Multilayered electrospun scaffolds for tendon tissue engineering. *Tissue Eng Part A.* 2013;19(23-24): 2594–2604.
38. Berglund M, Reno C, Hart DA, Wiig M. Patterns of mRNA expression for matrix molecules and growth factors in flexor tendon injury: differences in the regulation between tendon and tendon sheath. *J Hand Surg Am.* 2006;31(8): 1279–1287.
39. Dunkman AA, Buckley MR, Mienaltowski MJ, Adams SM, Thomas SJ, Satchell L, Kumar A, Pathmanathan L, Beason DP, Iozzo RV, Birk DE, et al. The tendon injury response is influenced by decorin and biglycan. *Ann Biomed Eng.* 2014; 42(3):619–630.
40. Su W, Qi W, Li X, Zhao S, Jiang J, Zhao J. Effect of Suture Absorbability on Rotator Cuff Healing in a Rabbit Rotator Cuff Repair Model. *Am J Sports Med.* 2018;46(11): 2743–2754.